Journal of Molecular Liquids 242 (2017) 364–374

Contents lists available at ScienceDirect

Journal of Molecular Liquids

journal homepage: www.elsevier.com/locate/molliq

Hydrothermal tuning of the morphology and crystallite size of zeolite nanostructures for simultaneous adsorption and photocatalytic degradation of methylene blue dye

Mostafa Y. Nassar *, Ehab A. Abdelrahman *

Chemistry Department, Faculty of Science, Benha University, Benha 13518, Egypt

ARTICLE INFO

Article history:
Received 11 June 2017
Received in revised form 6 July 2017
Accepted 11 July 2017
Available online 12 July 2017

Keywords:
Nanoparticles
Zeolites
Aluminum sources
Methylene blue dye
Adsorption
Photocatalytic degradation

ABSTRACT

We herein have reported on tuning of the morphology and crystallite size of the hydrothermally prepared zeolite nanostructures by using different aluminum sources. The investigation revealed that aluminum sulfate and aluminum chloride precursors produced non-crystalline forms, while aluminum isopropoxide, alumina, and aluminum metal precursors generated analcime nanoparticles with crystallite size of ca. 94.79, 112.57, and 105.87 nm, respectively. However, sodium aluminate precursor gave a mixture of analcime and nacrite phases with a crystallite size of ca. 77.95 nm. The as-prepared nanostructures were identified using XRD, FT-IR, FE-SEM, EDS, UV–Vis spectroscopy and BET surface area. The results exhibited that the direct optical energy gaps (E_g) and BET surface area were found to be (3.29 eV and 20.18 m^2/g), (3.15 eV and 16.28 m^2/g), (3.21 eV and 18.67 m^2/g), and (2.69 eV and 17.82 m^2/g) for the zeolite products prepared using aluminum isopropoxide, sodium aluminate, alumina, and aluminum metal precursors, respectively. The results also showed that the as-prepared zeolite nanostructures could be simultaneously used as adsorbents and photocatalysts for the removal of methylene blue (MB) dye from aqueous solutions. The adsorption of methylene blue dye over the zeolite adsorbents obeys pseudo-second-order model and intra-particle diffusion model. Interestingly, zeolite photocatalyst prepared using aluminum isopropoxide degraded the MB dye with percentage of 85% and 100% within 180 and 110 min in the presence of UV and (UV + H_2O_2), respectively. The degradation processes followed the pseudo-first-order model. The prepared zeolites are proposed as promising candidates for the removal of MB from aqueous media.

1. Introduction

Zeolites are a crystalline material consist of silicon and aluminum metals which were arranged in tetrahedral shape TO_4 (T = Si, Al), where oxygen atoms connect neighboring tetrahedral [1]. In the zeolite framework, Al^{3+} replaces some of Si^{4+} in SiO_2 network, creating a negative charge on zeolite which is neutralized by positive ions such as NH_4^+, Na^+ and K^+. These ions can be easily replaced by other ions; hence, this gives zeolites the characteristics and features which make them unique materials. The term zeolite was launched in the eighteenth century by Axel Fredrick (Swedish scientist) who was interested in metals. Zeolites have multiple applications in various fields. In the agricultural field: zeolites are used as fertilizer owing to their ability in ammonia exchange and absorption of excess water from the soil, then zeolites deliver this to the plant slowly, preventing root rot and reducing drought. Zeolites are also used in poultry farms to improve the efficiency of feeds and get rid of unwanted smells and strengthen immunity birds due to their high ability to remove ammonia which can cause blindness to poultry [2–10]. In the industrial field: zeolites are used in various applications such as fluid catalytic cracking, cement industry (because zeolites can reduce required heat during the manufacturing process; consequently, can reduce both fuel consumption and rising gas such as CO_2 and SO_2), natural gas purification in wells and oil refineries (due to their ability of removing CO_2 and SO_2 gases), chemical detergents industry, ceramics and porcelain industry, as well as electronics and sustainable production of hydrogen via water splitting [9–18]. In the environmental field: due to the toxicity of organic and inorganic pollutants, researchers have devoted much of their work to removing of pollutants [19–30]. Owing to the ability of zeolites to adsorb organic and inorganic pollutants in addition to its semiconducting properties, those materials are used in water treatment. Zeolites can be used as adsorbents and photocatalysts to degrade different organic pollutants [30–33]. Natural zeolite found in nature in basaltic rocks and sediments that formed through the ages by the hot mineral water. Due to the scarcity of natural zeolites, scientists have devoted their effort to preparing

* Corresponding authors. Tel.: +20106872555; Tel.: +201010636875.
E-mail addresses: m_y_nassar@yahoo.com, m_y_nassar@fsc.bu.edu.eg (M.Y. Nassar), dr.ehabsaleh@yahoo.com, ehab.abdelrahman@fsc.bu.edu.eg (E.A. Abdelrahman).

http://dx.doi.org/10.1016/j.molliq.2017.07.033
0167-7322/

those materials industrially. Analcime is considered to be one of the most important types of industrial zeolites attributing to its vast applications such as membrane for fuel cells [34], separation of surfactant [35], removal of inorganic pollutants (such as SO_4^{2-}, Cu^{2+}, Cs^{+}, Sr^{2+}, and arsenic) and organic pollutants (such as methylene blue dye and tetracycline) [36–41]. It can be also used in oxidation of organic compounds such as formaldehyde, benzyl alcohol and cyclohexane [42–44]. Hydrothermal route proved its efficiency in synthesis of various metal oxides [20,45–47]. Therefore, this route has been adopted to prepare analcime either in presence of template (such as tetraethyl ammonium bromide, tetrapropyl ammonium hydroxide and ethylene diamine derivatives) [48–50] or in absence of organic template [51–55]. It is well-known that aluminum sources play a crucial role in the zeolite properties such as crystal size, surface area, morphology, Si/Al ratio and have no effect on the type of zeolite phase under the same preparation conditions [56]. Therefore, this discussion stimulated us to prepare zeolite nanostructures with smaller crystallite size and different phases using more facile route.

Herein, we have developed a new strategy to synthesize zeolite nanostructures with different phases and crystallite sizes using a hydrothermal route. Therefore, we have investigated the effect of aluminum sources such as aluminum sulfate, aluminum chloride, aluminum isopropoxide, sodium aluminate, alumina, and aluminum metal precursors on the type of zeolite phases, as well as on their crystal size, surface area, and morphology. The as-prepared zeolite products were identified using several techniques. Moreover, the as-prepared zeolite compounds were applied to remove methylene blue dye from aqueous solutions. The as-fabricated zeolites were used as adsorbents and photocatalysts, simultaneously, for the first time, to the best of our knowledge. The photocatalytic properties of the as-prepared zeolites were investigated in the absence and presence of H_2O_2 under UV illuminations.

2. Experimental

2.1. Materials and reagents

All chemical used in the current investigation were of analytical grade and employed as received without further purification: The chemicals: sodium hydroxide pellets (NaOH), aluminum sulfate ($Al_2(SO_4)_3.18H_2O$), aluminum chloride ($AlCl_3.6H_2O$), aluminum isopropoxide ($Al(OCH(CH_3)_2)_3$), sodium aluminate ($NaAlO_2$), alumina (Al_2O_3), aluminum metal, Ludox AS30 colloidal silica (SiO_2, 30% suspension in H_2O), and methylene blue dye (MB; $C_{16}H_{18}ClN_3S$), were supplied by Sigma-Aldrich Chemical Company.

2.2. Preparation of zeolites using different aluminum sources

The zeolite products were prepared hydrothermally as follows: 7.72 g sodium hydroxide (0.193 mol) and an appropriate weight of an aluminum source [10.66, 7.73, 6.54, 2.62, 1.63, or 0.86 g of aluminum sulfate, aluminum chloride, aluminum isopropoxide, sodium aluminate, alumina or aluminum metal, respectively], so as to give 0.032 mol of aluminum cations, were dissolved in 69.5 mL deionized water in a Pyrex beaker. Afterward, 50 g of Ludox AS30 colloidal silica was dropwise added to the previously prepared aluminum solution under vigorous stirring. The reaction blend was stirred until it turned into gel. Then, the reaction blend was left for aging at room temperature (~25 °C) for 20 h. Therefore, the molar composition of the produced synthesis gel was $125SiO_2{:}8Al_2O_3$. After that the reaction mixture was transferred into a Teflon-lined stainless steel autoclave set up at 180 °C for 5 days, in an electric oven. After completion of the hydrothermal reaction, the autoclave was then allowed to naturally cooled, and the precipitated product was collected by centrifugation. The zeolite samples were washed with water then with ethanol several times, and dried at 120 °C overnight in an oven.

2.3. Simultaneous adsorption and photocatalytic degradation of methylene blue dye

In a typical adsorption experiment, in Erlenmeyer flasks, 0.1 g of adsorbent (prepared using aluminum isopropoxide or sodium aluminate) was stirred with 50 mL of methylene blue dye solution (with an initial concentration of 10 mg/L) at 500 rpm for different interval times in dark place and at room temperature (~25 °C). At pre-defined time intervals, aliquots were withdrawn out of the flasks and centrifuged to separate the suspension zeolites. The remaining dye concentration in the

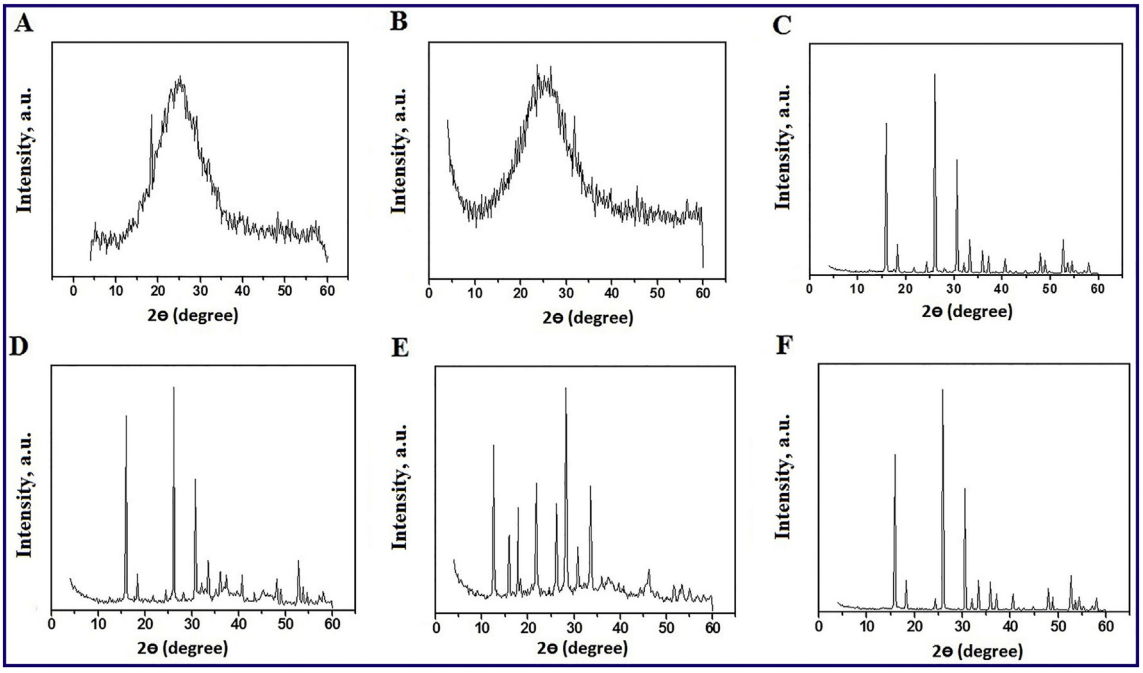

Fig. 1. XRD patterns of the as-prepared zeolite products fabricated using: (A) aluminum sulfate, (B) aluminum chloride, (C) aluminum isopropoxide, (D) sodium aluminate, (E) alumina, and (F) aluminum metal precursors.

Table 1
Outline of XRD, SEM, BET, and EDS results for the as-prepared zeolites.

Aluminum precursor	XRD		SEM		Surface study		Weight % of elements			
	Phase	Crystallite size (nm)	Shape	Particle size (μm)	BET area (m^2/g)	Total pore volume (cc/g)	O	Na	Al	Si
Aluminum sulfate	Amorphous	–	–	–	–	–	–	–	–	–
Aluminum chloride	Amorphous	–	–	–	–	–	–	–	–	–
Aluminum isopropoxide	Analcime	94.79	Spherical	17.00	20.18	0.012	52.41	7.43	10.06	30.09
Sodium aluminate	Analcime and nacrite	77.95	Irregular and spherical	4.00	16.28	0.015	55.42	2.44	32.71	9.44
Alumina	Analcime	112.57	Irregular and spherical	3.50	18.67	0.017	58.70	7.95	8.27	25.07
Aluminum metal	Analcime	105.87	Spherical	3.00	17.82	0.014	54.08	7.98	9.51	28.43

supernatant was determined employing an UV–Vis spectrophotometer at 663 nm wavelength. Afterward, when adsorption reached its maximum (i.e. equilibrium adsorption time), the degradation process of MB dye was investigated in the absence and presence of 2 mL of 0.5 M hydrogen peroxide solution under UV illumination using UV lamps (Philips at 365 nm 4 × 20 watt). After separating the catalyst by centrifugation, the absorption of the supernatant was measured at 663 nm at different time intervals using an UV–Vis spectrophotometer. % removal or degradation of methylene blue dye can be calculated using Eq. (1).

$$\% \text{ Removal or degradation} = [(C_i - C_f)/C_i]100 \quad (1)$$

where, C_i (mg/L) is the initial concentration of MB dye (in case of adsorption process) or concentration of methylene blue dye after attaining equilibrium adsorption time in the dark (in case of photocatalytic degradation), C_f (mg/L) is the final concentration of MB dye solution after adsorption or photocatalytic degradation. The adsorption capacity of the adsorbents Q (mg/g) can be calculated using Eq. (2).

$$Q = (C_i - C_f)V/m \quad (2)$$

where, V (L) is the volume of the dye solution, and m (g) is the mass of the adsorbents.

2.4. Physico-chemical measurements

The XRD patterns of the prepared samples were collected on a 18 kW diffractometer (Bruker; model D8 Advance) with monochromated Cu Kα radiation (λ) 1.54178 Å. FT-IR spectra were recorded on a Nicolet iSio FT-IR spectrophotometer in the 4000–400 cm^{-1} region using the KBr disk technique. The FE-SEM images of the as-fabricated products were collected using a field emission scanning electron microscope (FE-SEM; JEOL, model JSM-6390). Elemental analysis was carried out using link, ISIS-300, Oxford EDS (energy dispersion spectroscopy) detector. The BET (Brunauer-Emmet-Teller) surface area and pore size of the as-produced products were estimated employing nitrogen gas adsorption isotherms on Quantachrome analyzer (Nova 2000 series, USA) at 77 K. The adsorption and/or degradation investigation were performed using an UV–Vis spectrophotometer (Jasco; model V530).

3. Results and discussion

3.1. XRD and surface texture studies

XRD patterns of the as-synthesized samples produced using aluminum sulfate, aluminum chloride, aluminum isopropoxide, sodium aluminate, alumina and aluminum metal are depicted in Fig. 1(A–F), respectively. It was found that the products prepared using aluminum sulfate and aluminum chloride were amorphous owing to the broad band appeared at 2θ = 20–40°. Whereas, the samples synthesized using aluminum isopropoxide, alumina, and aluminum metal were analcime phase because of the appearance of peaks at 2θ = 16, 18, 26 and 31–50° which can be perfectly indexed into the monoclinic type phase with cell constants: a = 13.689 Å, b = 13.676 Å and c = 13.665 Å (space group Cmcm, JCPDS card 86-2455) [57]. The intense peaks

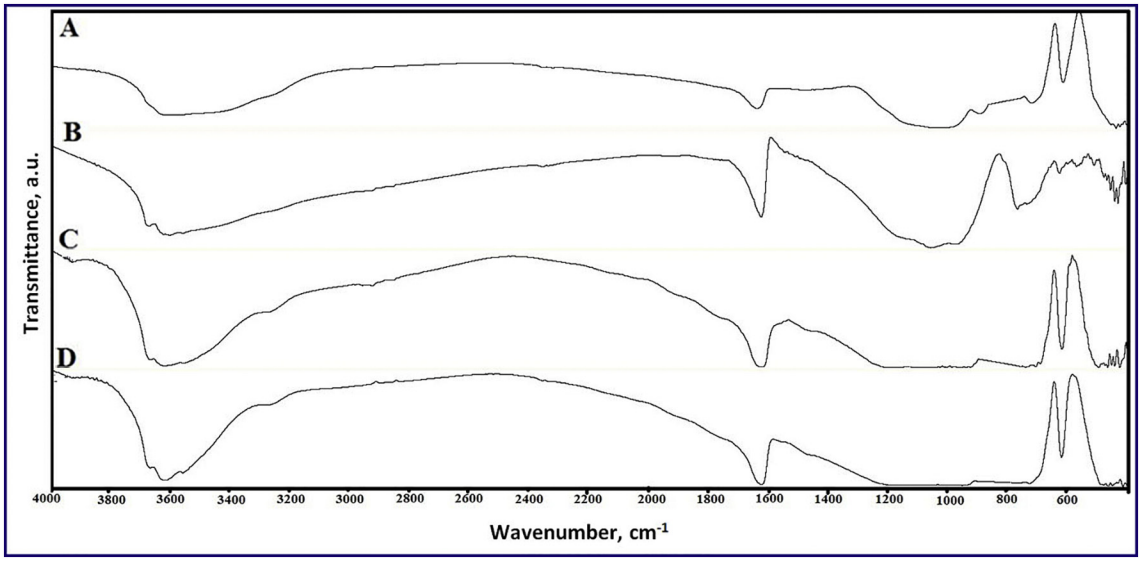

Fig. 2. FT-IR spectra of the as-prepared zeolite products fabricated using: (A) aluminum isopropoxide, (B) sodium aluminate, (C) alumina, and (D) aluminum metal precursors.

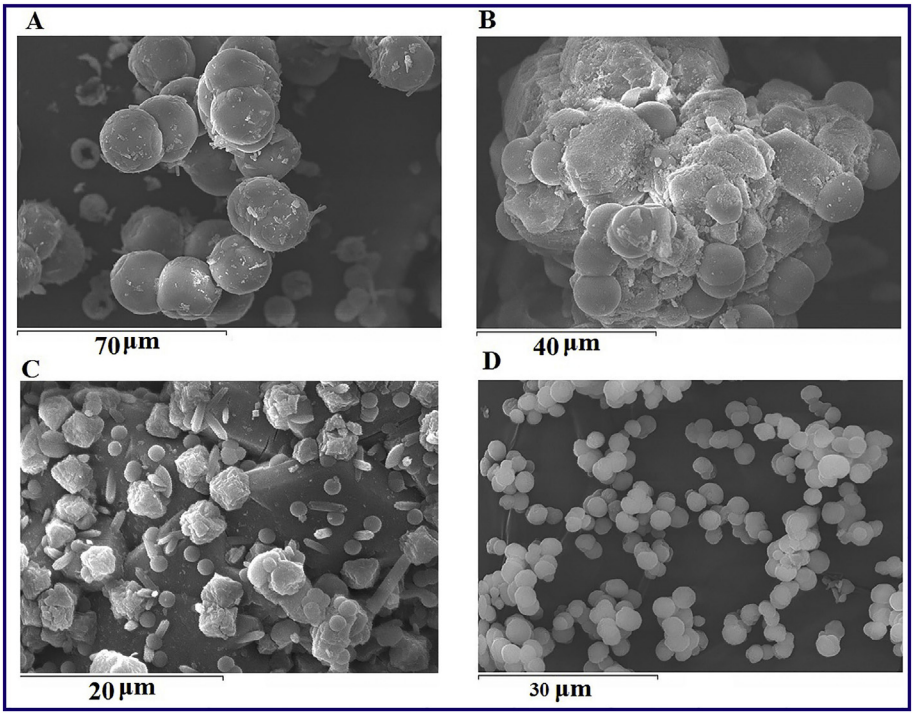

Fig. 3. FE-SEM images the as-prepared zeolite products fabricated using: (A) aluminum isopropoxide, (B) sodium aluminate, (C) alumina, and (D) aluminum metal precursors.

appeared at 2θ = 12, 22 and 28 in along with the peaks of analcime for the sample obtained using sodium aluminate confirmed the presence of nacrite zeolite phase. This phase can be perfectly indexed into the monoclinic type phase with cell constants: a = 13.689 Å, b = 13.676 Å and c = 13.665 Å (space group Cmcm, JCPDS card 76-1781) [58]. Thus, we can conclude that aluminum sources can influence on zeolite phase products. Moreover, the acidic counter ion of aluminum source exhibited a significant effect on the type and crystallization of zeolite phase. It is well-known that aluminum sources play a significant role in the zeolite properties such as crystal size, surface area, morphology, Si/Al ratio. And, they have no effect on the type of zeolite phase under the same experimental conditions [56]. However, this study exhibited that aluminum sources played a crucial role in production of zeolites. This is based on that various phases of zeolites could be produced by changing aluminum sources.

The average crystallite size was estimated using the Debye–Scherrer formula (Eq. (3)):

$$D = 0.9\lambda/\beta\cos\theta_B \quad (3)$$

where, λ, β, θ_B are the X-ray wavelength, full width at half maximum (FWHM) of the diffraction peak, and Bragg diffraction angle,

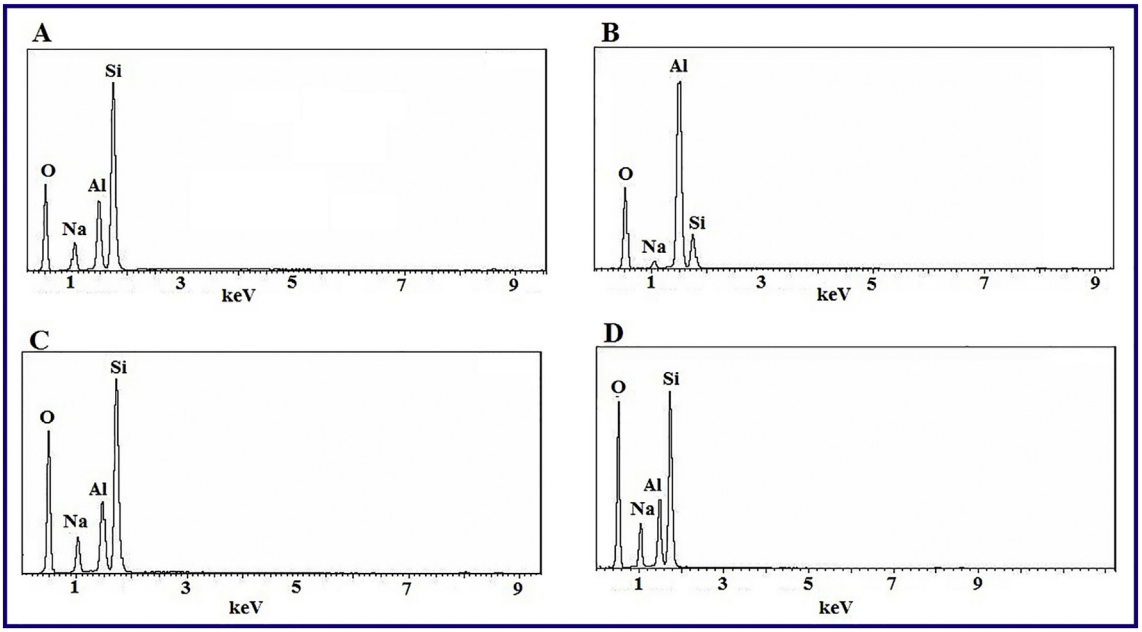

Fig. 4. EDS spectra of the as-prepared zeolite products fabricated using: (A) aluminum isopropoxide, (B) sodium aluminate, (C) alumina, and (D) aluminum metal precursors.

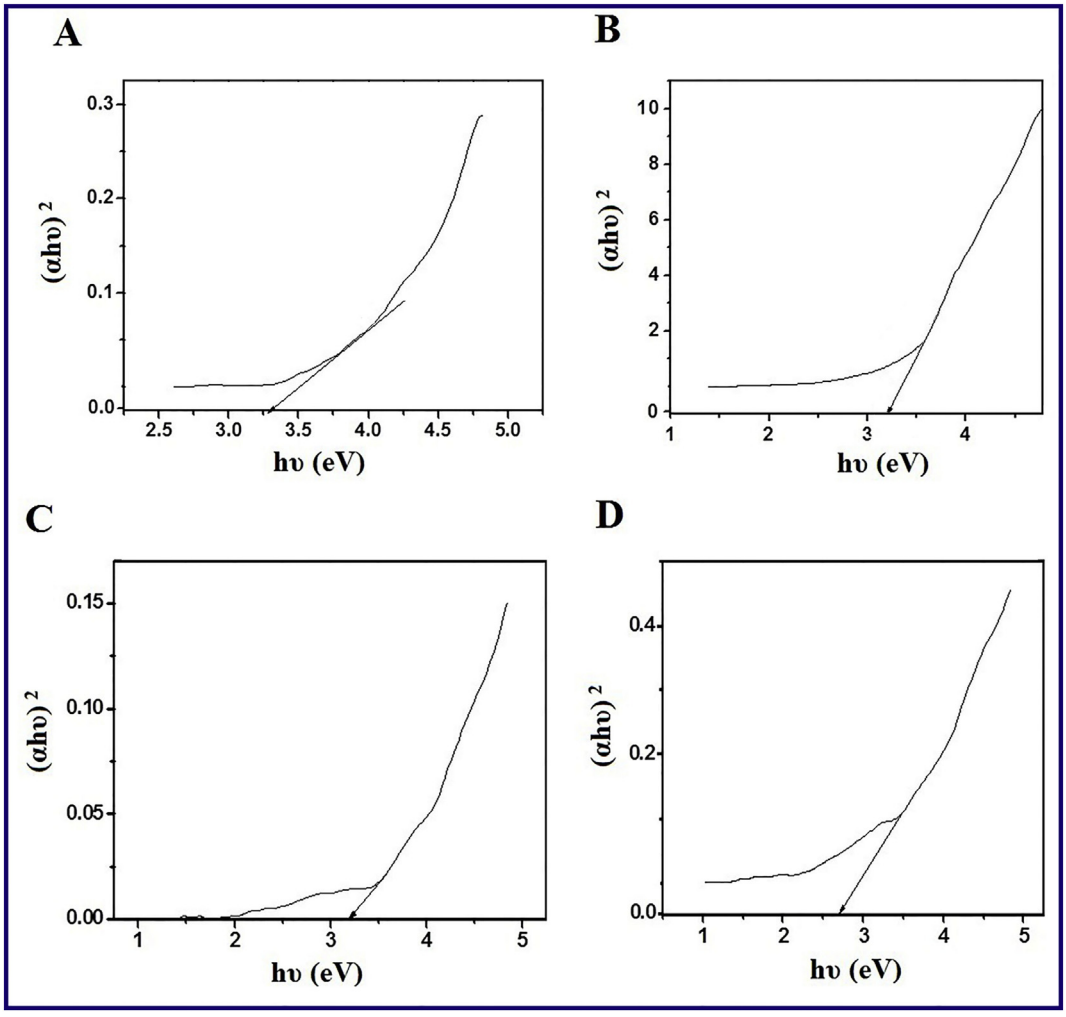

Fig. 5. Plots of $(\alpha h\upsilon)^2$ versus hυ of the as-prepared zeolite products fabricated using: (A) aluminum isopropoxide, (B) sodium aluminate, (C) alumina, and (D) aluminum metal precursors.

respectively. The XRD data revealed that the average crystallite sizes of zeolite nanostructures were found to be 94.79, 77.95, 112.57 and 105.87 nm for products prepared using aluminum isopropoxide, sodium aluminate, alumina and aluminum metal, respectively, as presented in Table 1.

The textural characteristics such as surface area and pore volume were evaluated from the low temperature nitrogen adsorption and summarized in Table 1. The BET surface area was found to be 20.18, 16.28, 18.67 and 17.82 m^2/g, respectively; whereas, total pore volume was found to be 0.012, 0.015, 0.017 and 0.014 cc/g, respectively.

3.2. FT-IR studies

The FT-IR transmission spectra for samples prepared using aluminum isopropoxide, sodium aluminate, alumina and aluminum metal are shown in Fig. 2(A–D), respectively. Notably, all products revealed similar vibrational absorption bands. The bands appeared at about 1032 cm^{-1} may be attributed to the asymmetric stretching vibration of T—O (T = Si, Al). Those appeared at about 630 cm^{-1} may be assigned to M—O bond [59,60] and in the current case they can be attributed to T—O—T (T = Si, Al) symmetric stretching vibration. The bands appeared near 452 cm^{-1} may be due to T—O—T (T = Si, Al) bending vibration [61]. The bands appeared at about 3617 and 1637 cm^{-1} can be attributed to stretching and bending vibration of surface adsorbed zeolite water, respectively [62–66].

3.3. SEM and EDS studies

Fig. 3(A–D) shows FE-SEM images of the samples prepared using aluminum isopropoxide, sodium aluminate, alumina and aluminum metal, respectively. The results showed that the zeolites, prepared using aluminum isopropoxide and aluminum metal, are composed of spherical shapes with an average particle size of 17 and 3 μm, respectively, as outlined in Table 1. However, the zeolite products synthesized

Table 2
Optical energy gap, refractive index, limiting dielectric constant, linear optical susceptibility, and reflectivity for the as-prepared zeolite samples.

Aluminum precursor used for zeolite preparation	E_g (eV)	Tripathy				Moss				Ravindra				Herve-Vandamme			
		n	ϵ_∞	χ	R	n	ϵ_∞	χ	R	n	ϵ_∞	χ	R	n	ϵ_∞	χ	R
Aluminum isopropoxide	3.29	2.31	5.32	4.32	0.16	2.32	5.37	4.37	0.16	2.01	4.18	3.18	0.11	2.25	5.04	4.04	0.15
Sodium aluminate	3.15	2.36	5.57	4.47	0.16	2.35	5.52	4.52	0.16	2.15	4.63	3.63	0.13	2.29	5.26	4.26	0.15
Alumina	3.21	2.63	6.90	5.90	0.20	2.49	6.23	5.23	0.18	2.56	6.58	5.58	0.19	2.51	6.28	5.28	0.19
Aluminum metal	2.69	3.03	9.16	8.16	0.25	2.72	7.35	6.35	0.21	2.99	8.97	7.97	0.25	2.78	7.77	6.77	0.22

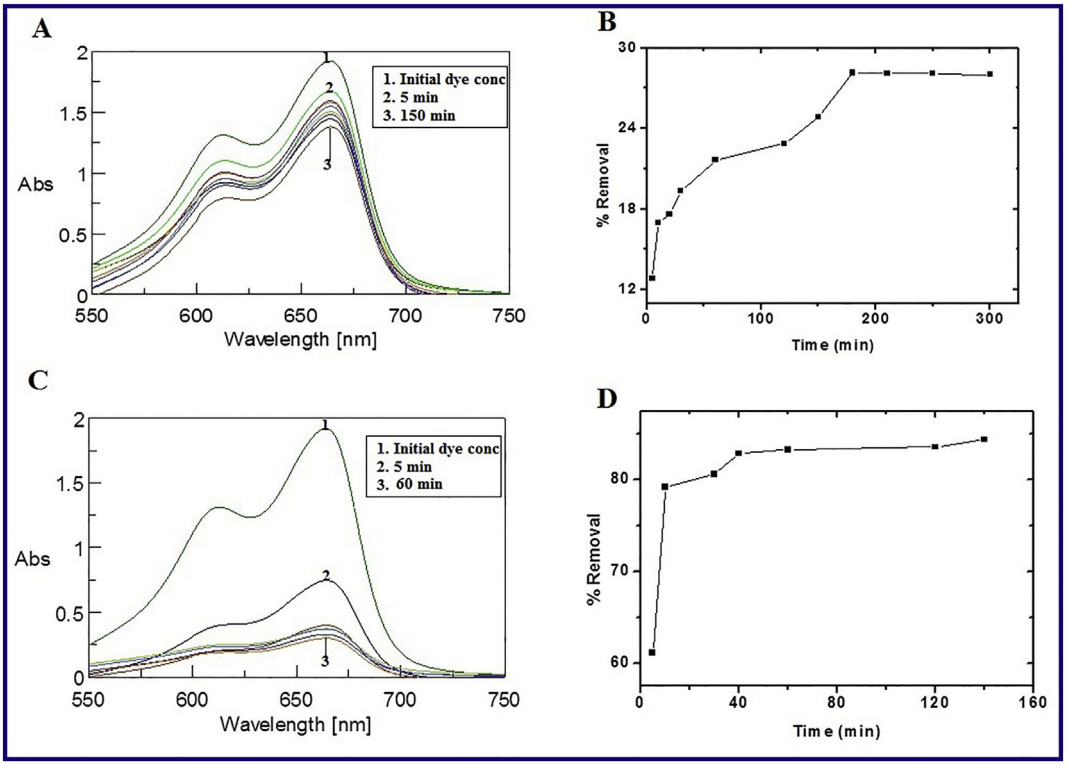

Fig. 6. Adsorption of methylene blue dye onto zeolite sample prepared using aluminum isopropoxide (A, B), and sodium aluminate (C, D) precursors.

using sodium aluminate and alumina are composed of spherical and irregular shapes with an average particle size of 4 and 3.5 μm, respectively, as presented in Table 1. Fig. 4(A–D) depicts EDS spectra of the as-prepared zeolites. The results indicated that all the as-synthesized samples are composed of Si, Al, Na and O as summarized in Table 1. The Si/Al molar ratio of the samples prepared using aluminum isopropoxide, sodium aluminate, alumina and aluminum metal were found to be 2.99, 0.29, 3.03 and 2.99, respectively.

3.4. Optical properties of the as-prepared zeolite products

The optical properties of the as-prepared zeolite nanostructures have been investigated by calculating the values of E_g, n, ϵ_∞, χ and R: where, E_g (eV) is an optical energy gap, n is a refractive index of substance (a measure of its transparency to the incident photons), ϵ_∞ is a limiting dielectric constant (the ratio of the permittivity of a substance to that of free space or vacuum) describing the response of the

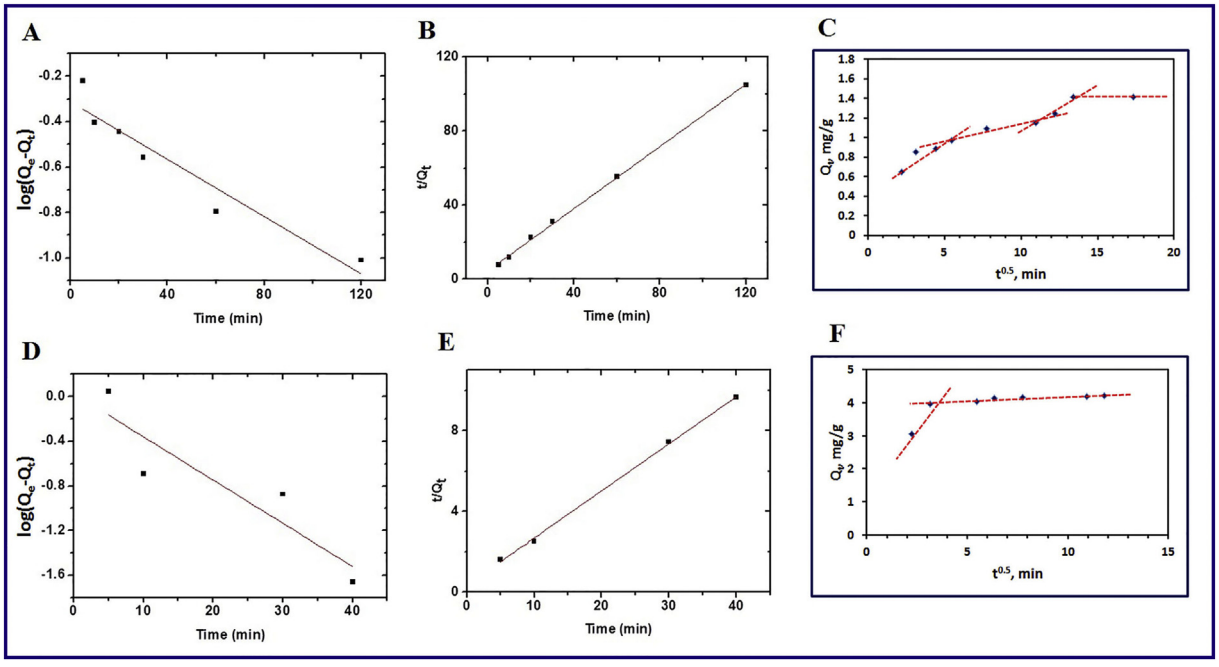

Fig. 7. Pseudo-first-order (A, D), pseudo-second-order (B, E), and intra particle diffusion model (C, F) for the adsorption of MB dye on the zeolite product prepared using aluminum isopropoxide and sodium aluminate precursors, respectively.

Table 3
Calculated constants of pseudo-first-order, pseudo-second-order, and intra particle diffusion model for the as-prepared zeolite samples.

Aluminum precursor used for zeolite preparation	Pseudo first order			Pseudo second order			Intra particle diffusion model		
	R^2	Q_e (mg/g)	K_1 (min^{-1})	R^2	Q_e (mg/g)	K_2 (g/mg·min)	R^2	K_{int} (mg/(g·$min^{0.5}$))	C (mg/g)
Aluminum isopropoxide	0.89	0.49	0.0063	0.99	1.19	0.1521	0.63	0.0521	0.6316
Sodium aluminate	0.75	1.07	0.0387	0.99	4.28	0.1547	0.47	0.2096	2.8962

substance to the electromagnetic radiation mediated through the interaction of photons and electrons, χ is linear optical susceptibility, and R is reflectivity (defined through the ratio of the reflected power to incident power) and it describes the optical response of the surface of a substance.

UV–Vis absorption spectra of the as-prepared zeolite nanostructures were performed in nujol mull in order to estimate their optical energy gap. The optical energy gaps (E_g) [67] can be determined using Eq. (4).

$$(\alpha h\upsilon)^y = K(h\upsilon - E_g) \tag{4}$$

where, α, K, y are the absorption coefficient, a constant, and an integer equals either 2 for a direct allowed transitions or 1/2 for an indirect allowed transitions, respectively. We have plotted $(\alpha h\upsilon)^2$ versus hυ as shown in Fig. 5. It seems that direct allowed transitions are the predominant for the as-prepared zeolite products. The optical energy gaps (E_g) of the zeolite products were determined by extrapolating each graph so as $(\alpha h\upsilon)^2 = 0$. The optical energy gap values of the as-prepared zeolite products—prepared using aluminum isopropoxide, sodium aluminate, alumina and aluminum metal—were estimated to be 3.29, 3.15, 3.21, and 2.69 eV, respectively, as presented in Table 2. Moreover, the obtained energy gap values indicate the semiconducting properties of the as-prepared zeolite products [68]. The refractive index values (n) have been determined employing four different relationships: Tripathy (Eq. (5)), Moss (Eq. (6)), Ravindra (Eq. (7)) and Herve-Vandamme (Eq. (8)) [69].

$$n = n_o\left[1 + \alpha e^{-\beta E_g}\right] \tag{5}$$

$$n^4 E_g = 95 \tag{6}$$

$$n = 4.084 - 0.62\, E_g \tag{7}$$

$$n^2 = 1 + \left[\frac{A}{E_g + B}\right]^2 \tag{8}$$

where, $n_o = 1.73$, $\alpha = 1.9017\ eV^{-1}$, $\beta = 0.539\ eV^{-1}$, A is hydrogen ionization energy (= 13.6 eV), and B is a constant (the difference between UV resonance energy and band energy gap (= 3.47)). In addition, limiting dielectric constant (ϵ_∞), linear optical susceptibility (χ) and reflectivity (R) have been determined by utilizing Eqs. (9), (10), and (11), respectively.

$$\epsilon_\infty = n^2 \tag{9}$$

$$\chi = \epsilon_\infty - 1 \tag{10}$$

$$R = [(n-1)/(n+1)]^2 \tag{11}$$

The estimated optical properties have been presented in Table 2. It is noteworthy that this is considered to be the first time to study the semiconductor properties of zeolites. Therefore, this opens up the possibility to use those materials as photocatalyst in photocatalytic degradation of organic dyes in aqueous solutions.

4. Simultaneous adsorption-photocatalytic degradation of methylene blue dye

The dual adsorption and **photocatalytic** degradation of methylene blue dye from aqueous solution have been investigated. In this light, based on the small crystallite size and high surface area, the as-prepared analcime phase (generated using aluminum isopropoxide) and the mixed phase of analcime and nacrite (prepared using sodium aluminate) have been used for this investigation. The effect of the contact time on the adsorption efficiency of the aforementioned zeolite

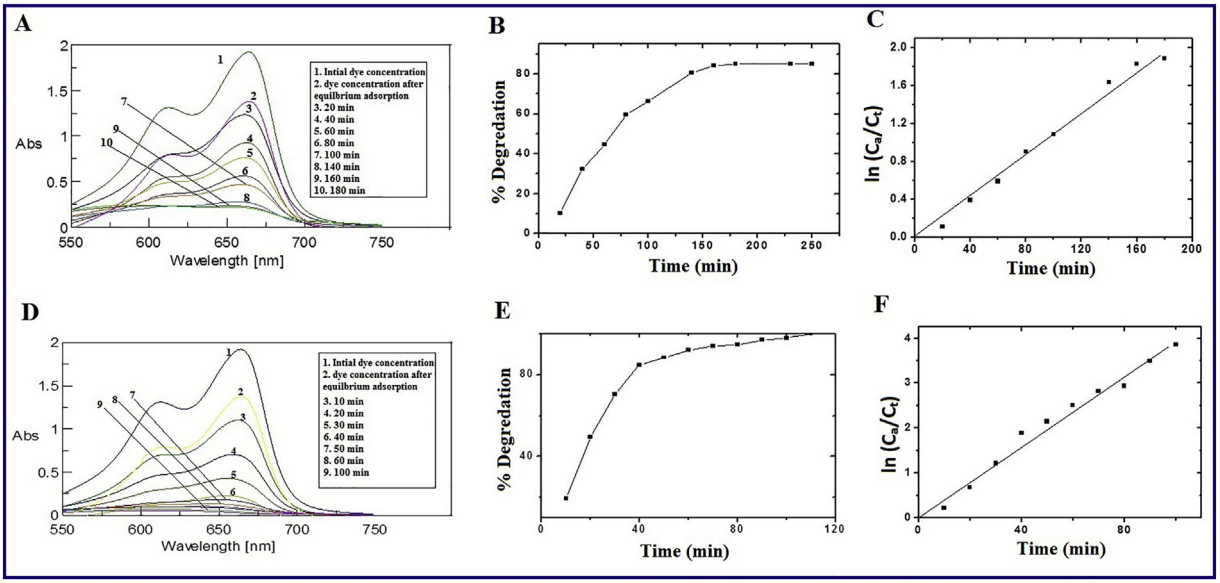

Fig. 8. Photocatalytic degradation of methylene blue dye over zeolite sample prepared using aluminum isopropoxide precursor under UV irradiation in the absence of H_2O_2 (A–C) and in the presence of H_2O_2 (D–F).

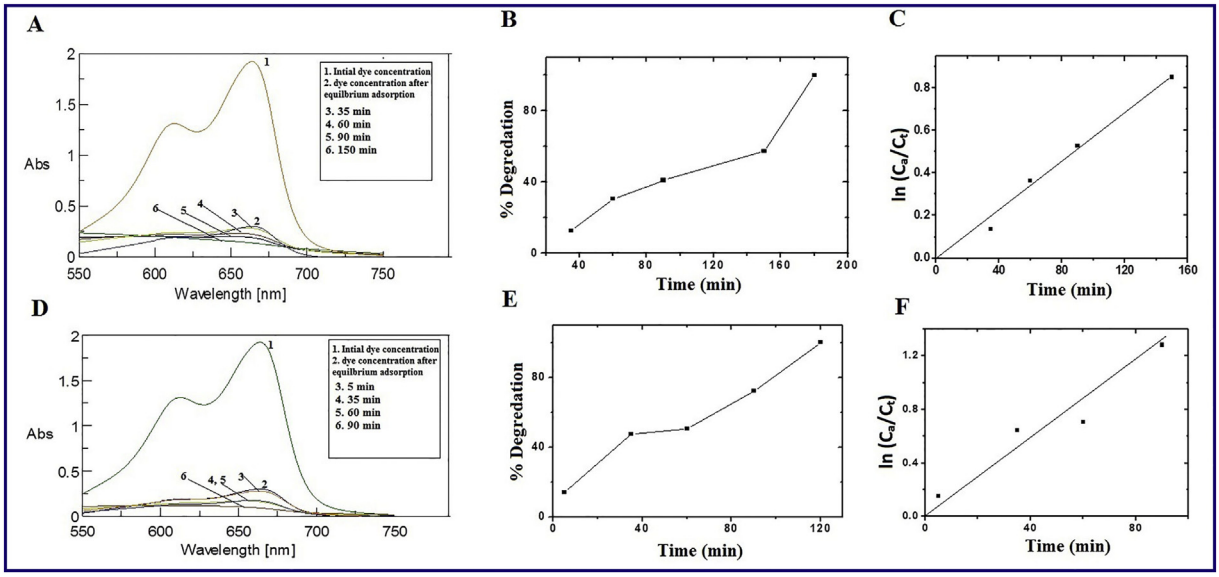

Fig. 9. Photocatalytic degradation of methylene blue dye over zeolite sample prepared using sodium aluminate precursor under UV irradiation in the absence of H_2O_2 (A–C) and in the presence of H_2O_2 (D–F).

adsorbents for the removal of methylene blue dye was examined under the experimental conditions: 0.1 g of adsorbents, 50 mL of MB dye with an initial concentration of 10 mg/L, at 25 °C. The results are displayed in Fig. 6(A) and (C), respectively. The data exhibited that the dye % removal using the as-prepared analcime zeolite enhanced rapidly until it reached ca. 24.85% in 150 min and the equilibrium state was attained, as shown in Fig. 6(B). The zeolite products, prepared using sodium aluminate precursor (i.e. a mixed phase of analcime and nacrite), % removal increased with increasing the contact time and reached 83.28% in only 60 min where the adsorption process attained the equilibrium state as depicted in Fig. 6(D). Notably, the equilibrium state was attained owing to saturation of active sites of the adsorbents at the equilibration time of adsorption. In addition, adsorption kinetics has a crucial role in the explanation of the adsorption mechanisms. Therefore, we have investigated adsorption of MB dye on the as-prepared zeolites using the following kinetic models: pseudo-first-order (Eq. (12)), pseudo-second-order (Eq. (13)) and intra-particle diffusion (Eq. (14)) [26].

$$\log(Q_e - Q_t) = \log Q_e - K_1 t/2.303 \tag{12}$$

$$t/Q_t = \left(1/K_2 Q_e^{\,2}\right) + (1/Q_e)t \tag{13}$$

$$Q_t = K_{int} t^{0.5} + C \tag{14}$$

where, Q_e (mg/g) is the adsorbed dye at equilibrium, Q_t (mg/g) is the adsorbed dye at time t (min), K_1 (1/min) is the pseudo-first-order rate constant of the adsorption process, K_2 (g/mg·min) is the pseudo-

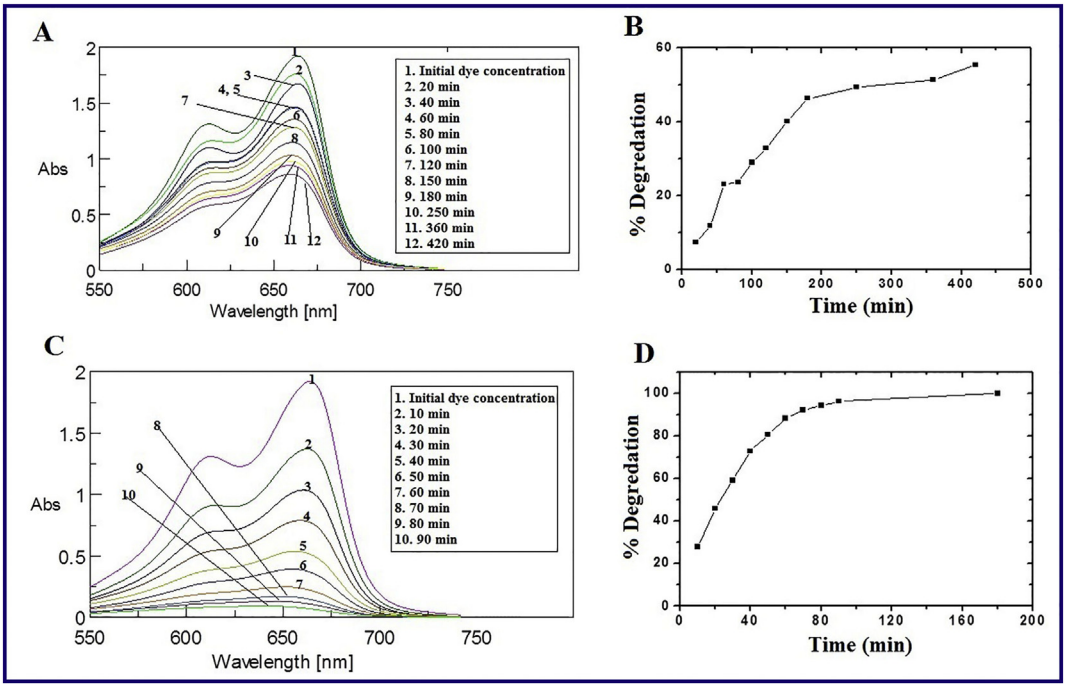

Fig. 10. Photocatalytic degradation of methylene blue dye without presence of any photocatalyst under UV irradiation in the absence of H_2O_2 (A, B) and in the presence of H_2O_2 (C, D).

Table 4
Kinetic parameters of the photocatalytic degradation of MB dye over the zeolites prepared using aluminum isopropoxide and sodium aluminate precursors under UV irradiation in the absence and presence of H_2O_2.

Aluminum precursor used for zeolite preparation	UV irradiation		UV irradiation + H_2O_2	
	R^2	K_{obs} (min^{-1})	R^2	K_{obs} (min^{-1})
Aluminum isopropoxide	0.998	0.012	0.99	0.037
Sodium aluminate	0.995	0.013	0.94	0.023

second-order rate constant of the adsorption process, C (mg/g) is the thickness of boundary layer, and K_{int} (mg/(g·$min^{0.5}$)) is internal diffusion constant. K_1 and $Q_{e(cal)}$ values in (Eq. (12)) were determined by plotting $\log(Q_e - Q_t)$ versus t, as shown in Fig. 7(A, D). Besides, K_2 and $Q_{e(cal)}$ values were calculated utilizing the plot of t/Q_t against t (Fig. 7(B, E)), and K_{int} and C values were estimated from the plot of Q_t versus $t^{0.5}$ (Fig. 7(C, F)). The estimated kinetic parameters of the adsorption of MB dye on the as-prepared zeolites are listed in Table 3. The obtained results revealed that the adsorption of methylene blue dye over the zeolite adsorbents followed pseudo-second-order model because the value of the correlation coefficients ($R^2 = 0.99$) was close to unity compared to those obtained from the pseudo-first-order model ($R^2 = 0.89$ and 0.75) (Fig. 7(B, E)). Moreover, the fitness of pseudo-second-order model for describing the adsorption data was supported from the closeness of the calculated and experimental adsorption capacity as listed in Table 3. The intra-particle diffusion model supposes that the rate-controlling process is diffusion within the particles (inner diffusion of adsorbed molecules or ions inside the adsorbents during the adsorption process). In addition, zero intercepts of the plot of Q_t against $t^{0.5}$ support the validity of this model. In the current investigation, plot of Q_t versus $t^{0.5}$ produced linear fitting which did not pass through the origin (Fig. 7(C, F))), referring to that intra-particle diffusion was not the only rate-controlling mechanism of methylene blue dye adsorption. However, the adsorption mechanism of methylene blue dye on the zeolite adsorbent was also controlled by some other mechanisms such as film diffusion and bulk diffusion [25,26].

Furthermore, the photocatalytic activity of the as-synthesized zeolites for the degradation of MB dye has been examined after attaining the adsorption-desorption equilibrium, as mentioned before. The photocatalytic degradation of MB dye over the as-synthesized zeolite photocatalysts was performed under UV irradiation. The results are displayed in Fig. 8(A, B, C) and (D, E, F), for the zeolite products prepared using aluminum isopropoxide and sodium aluminate precursors, respectively. The results revealed that zeolite photocatalyst prepared using aluminum isopropoxide precursor degraded MB dye under UV illumination. The photocatalytic degradation percentage, under UV illumination, reached about 85% within 180 min and 100% within 110 min in the absence and presence of H_2O_2, respectively, as shown in Fig. 8. It was noted that the percentage of 85% remained constant with increasing irradiation time because the degraded compounds might block the effect of UV light.

On the other hand, the photocatalytic degradation efficiency of the zeolite product, prepared using sodium aluminate, reached about 100% within 180 and 120 min in the absence and presence of H_2O_2, respectively, as displayed in Fig. 9(A–F). Notably, degradation of MB dye was also investigated in the absence of the as-prepared photocatalysts under UV illumination in the absence and presence of H_2O_2 and the results were depicted in Fig. 10(A–D). It was noticed that the degradation efficiency was higher and faster in the presence of the as-prepared zeolite materials.

Moreover, the photocatalytic degradation of MB dye over the as-prepared zeolite photocatalysts was quantitatively examined using the pseudo-first-order kinetic model (Eq. (15)), and the observed first-order rate constant (K_{obs}, 1/min) was calculated [21].

$$\ln(C_a/C_t) = (K_{obs})t \tag{15}$$

where, C_t (mg/L) is the remaining dye concentration at irradiation time t and C_a (mg/L) is the dye concentration after the adsorption equilibrium. Plotting $\ln(C_a/C_t)$ against t of the photocatalytic degradation data are displayed in Fig. 8(C, F) and Fig. 9(C, F), for the zeolite photocatalysts prepared using aluminum isopropoxide and sodium aluminate precursors, respectively. The calculated K_{obs} constants for both aforementioned photocatalysts are presented in Table 4. The results exhibited that the as-prepared zeolite photocatalyst generated from aluminum isopropoxide has the highest catalytic activity with K_{obs} of 0.037 min^{-1} under UV illumination in the presence of H_2O_2.

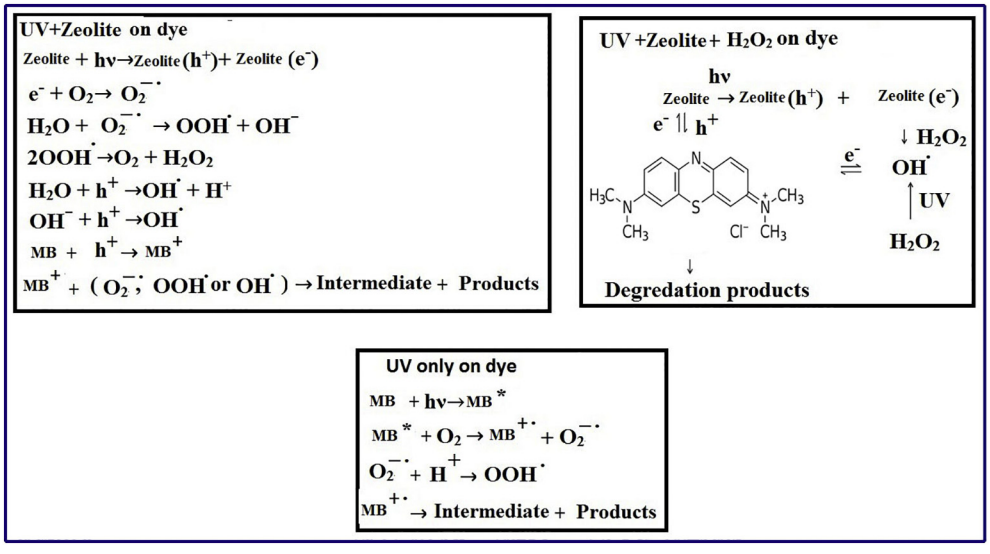

Scheme 1. Proposed reactions of the photodegradation of MB dye in the presence of (UV only), (Zeolite + UV), and (Zeolite + H2O2 + UV).

In addition, the mechanism of photo-degradation process using UV only, (Zeolite + UV), and (UV + eolite + H_2O_2) has been depicted in Scheme 1. The excited methylene blue dye molecules will convert O_2 to O_2• when the dye molecules absorb UV-light. Then, the produced O_2• radicals may react with protons (generated from the autoprotolysis of water) to generate superoxide radicals, **OOH•**. Afterward, those produced radicals may eventually degrade MB dye molecules completely to carbon dioxide, water, and mineral acids [21]. Photocatalytic degradation of methylene blue dye molecules in the presence of zeolite, under UV illumination, usually includes the separation of electron-hole pairs, generated on the surface of zeolite, and the subsequent reduction–oxidation reactions. The electrons can be scavenged by the adsorbed molecular oxygen species, and the holes can be trapped by water or adsorbed methylene blue molecules. Then, methylene blue dye molecules may be degraded directly by the influence of photo-generated oxidants. Furthermore, adding hydrogen peroxide in the presence of zeolite and UV may enhance the photo-degradation rate of methylene blue dye because the direct decomposition of hydrogen peroxide under UV light generating **OH•** radicals which directly may oxidize methylene blue dye molecules to carbon dioxide, water, and mineral acids, as shown in Scheme 1.

5. Conclusion

Different zeolite nanostructures have been prepared using a hydrothermal treatment of different aluminum precursors and Ludox AS30 colloidal silica. In this light, we have tuned the morphology, produced phase, and crystallite size of the zeolite products using different aluminum sources such as aluminum sulfate, aluminum chloride, aluminum isopropoxide, alumina, aluminum metal, and sodium aluminate. Interestingly, aluminum isopropoxide, alumina and aluminum metal precursors produced analcime phase while sodium aluminate generated a mixture of analcime and nacrite phases under the hydrothermal treatment of interest. The produced products have different morphologies and particle sizes based on the used aluminum precursor. The calculated optical energy gaps (E_g) revealed the semiconducting properties of the produced zeolites. The zeolite products prepared using aluminum isopropoxide and sodium aluminate showed simultaneous adsorption and photocatalytic properties; therefore, those samples were proposed as good candidates for the removal of MB dye from aqueous media.

Acknowledgements

The authors are thankful to Benha University—Egypt.

References

[1] C. Colella, A.F. Gualtieri, Cronstedt's zeolite, Microporous Mesoporous Mater. 105 (2007) 213–221.
[2] N. Zwingmann, I.D.R. Mackinnon, R.J. Gilkes, Use of a zeolite synthesised from alkali treated kaolin as a K fertiliser: glasshouse experiments on leaching and uptake of K by wheat plants in sandy soil, Appl. Clay Sci. 53 (2011) 684–690.
[3] G.B. Nuernberg, M.A. Moreira, P.R. Ernani, J.A. Almeida, T.M. Maciel, Efficiency of basalt zeolite and Cuban zeolite to adsorb ammonia released from poultry litter, J. Environ. Manag. 183 (2016) 667–672.
[4] S.C. Espécie Bueno, M.B. Filho, P.S.G. de Almeida, J.C. Polidoro, F.L. Olivares, M.S. Sthel, H. Vargas, L. Mota, M.G. da Silva, Cuban zeolite as ammonium carrier in urea-based fertilizer pellets: photoacoustic-based sensor for monitoring N-ammonia losses by volatilization in aqueous solutions, Sensors Actuators B Chem. 212 (2015) 35–40.
[5] N.G. Turan, The effects of natural zeolite on salinity level of poultry litter compost, Bioresour. Technol. 99 (2008) 2097–2101.
[6] Z. Li, Use of surfactant-modified zeolite as fertilizer carriers to control nitrate release, Microporous Mesoporous Mater. 61 (2003) 181–188.
[7] D. Papaioannou, P.D. Katsoulos, N. Panousis, H. Karatzias, The role of natural and synthetic zeolites as feed additives on the prevention and/or the treatment of certain farm animal diseases: a review, Microporous Mesoporous Mater. 84 (2005) 161–170.
[8] A. Lateef, R. Nazir, N. Jamil, S. Alam, R. Shah, M.N. Khan, M. Saleem, Synthesis and characterization of zeolite based nano–composite: an environment friendly slow release fertilizer, Microporous Mesoporous Mater. 232 (2016) 174–183.
[9] T. Ennaert, J. Van Aelst, J. Dijkmans, R. De Clercq, W. Schutyser, M. Dusselier, D. Verboekend, B.F. Sels, Potential and challenges of zeolite chemistry in the catalytic conversion of biomass, Chem. Soc. Rev. 45 (2016) 584–611.
[10] B.M. Weckhuysen, J. Yu, Recent advances in zeolite chemistry and catalysis, Chem. Soc. Rev. 44 (2015) 7022–7024.
[11] B. Zhang, Q. Lin, Q. Zhang, K. Wu, W. Pu, M. Yang, Y. Wu, Catalytic hydrothermal liquefaction of Euglena sp. microalgae over zeolite catalysts for the production of bio-oil, RSC Adv. 7 (2017) 8944–8951.
[12] C. Xue, H. Zhu, T. Xu, E. Wang, B. Xiao, X. Liu, X. Hao, G. Guan, Zeolite cage-lock strategy for in situ synthesis of highly nitrogen-doped porous carbon for selective adsorption of carbon dioxide gas, RSC Adv. 7 (2017) 24195–24203.
[13] S. Dasgupta, S. Divekar, A. Arya, P. Gupta, R. Chauhan, S. Bhadauria, A. Hanif, M.O. Garg, A. Nanoti, A vapor phase adsorptive desulfurization process for producing ultra low sulphur diesel using NiY zeolite as a regenerable adsorbent, RSC Adv. 5 (2015) 56060–56066.
[14] A. Qurashi, M. Alhaffar, Z.H. Yamani, Hierarchical ZnO/zeolite nanostructures: synthesis, growth mechanism and hydrogen detection, RSC Adv. 5 (2015) 22570–22577.
[15] M. Jaymand, Conductive polymers/zeolite (nano-)composites: under-exploited materials, RSC Adv. 4 (2014) 33935–33954.
[16] A. Harabi, S. Kasrani, L. Foughali, I. Serradj, M.T. Benhassine, S. Kitouni, Effect of TiO2 additions on densification and mechanical properties of new mulltifunction resistant porcelains using economic raw materials, Ceram. Int. 43 (2017) 5547–5556.
[17] Y. Kocak, E. Tasci, U. Kaya, The effect of using natural zeolite on the properties and hydration characteristics of blended cements, Constr. Build. Mater. 47 (2013) 720–727.
[18] A.M. Cardoso, M.B. Horn, L.S. Ferret, C.M.N. Azevedo, M. Pires, Integrated synthesis of zeolites 4A and Na–P1 using coal fly ash for application in the formulation of detergents and swine wastewater treatment, J. Hazard. Mater. 287 (2015) 69–77.
[19] M.Y. Nassar, S. Abdallah, Facile controllable hydrothermal route for a porous CoMn2O4 nanostructure: synthesis, characterization, and textile dye removal from aqueous media, RSC Adv. 6 (2016) 84050–84067.
[20] M.Y. Nassar, I.S. Ahmed, Template-free hydrothermal derived cobalt oxide nanopowders: synthesis, characterization, and removal of organic dyes, Mater. Res. Bull. 47 (2012) 2638–2645.
[21] M.Y. Nassar, I.S. Ahmed, I. Samir, A novel synthetic route for magnesium aluminate (MgAl2O4) nanoparticles using sol–gel auto combustion method and their photocatalytic properties, Spectrochim. Acta A Mol. Biomol. Spectrosc. 131 (2014) 329–334.
[22] M.Y. Nassar, A.A. Ali, A.S. Amin, A facile Pechini sol-gel synthesis of TiO2/Zn2TiO2/ZnO/C nanocomposite: an efficient catalyst for the photocatalytic degradation of Orange G textile dye, RSC Adv. 7 (2017) 30411–30421.
[23] M.Y. Nassar, H.M. Aly, E.A. Abdelrahman, M.E. Moustafa, Synthesis, characterization, and biological activity of some novel Schiff bases and their Co(II) and Ni(II) complexes: a new route for Co3O4 and NiO nanoparticles for photocatalytic degradation of methylene blue dye, J. Mol. Struct. 1143 (2017) 462–471.
[24] M.Y. Nassar, H.M. Aly, M.E. Moustafa, E.A. Abdelrahman, Synthesis, characterization and biological activity of new 3-substitued-4-amino-5-hydrazino-1,2,4-triazole Schiff bases and their Cu(II) complexes: a new approach to CuO nanoparticles for photocatalytic degradation of methylene blue dye, J. Inorg. Organomet. Polym. Mater. (2017) 1–14.
[25] M.Y. Nassar, T.Y. Mohamed, I.S. Ahmed, N.M. Mohamed, M. Khatab, Hydrothermally synthesized Co3O4, α-Fe2O3, and CoFe2O4 nanostructures: efficient nano-adsorbents for the removal of orange G textile dye from aqueous media, J. Inorg. Organomet. Polym. Mater. (2017).
[26] M.Y. Nassar, T.Y. Mohamed, I.S. Ahmed, I. Samir, MgO nanostructure via a sol-gel combustion synthesis method using different fuels: an efficient nano-adsorbent for the removal of some anionic textile dyes, J. Mol. Liq. 225 (2017) 730–740.
[27] M.Y. Nassar, E.I. Ali, E.S. Zakaria, Tunable auto-combustion preparation of TiO2 nanostructures as efficient adsorbents for the removal of an anionic textile dye, RSC Adv. 7 (2017) 8034–8050.
[28] M. Mostafa, H.M. Saber, A.A. El-Sadek, M.Y. Nassar, Preparation and performance of 99Mo/99mTc chromatographic column generator based on zirconium molybdosilicate, Radiochim. Acta (2016) 257–265.
[29] M. Mostafa, H.M. Saber, A.A. El-Sadek, M.Y. Nassar, A.S. Amin, Sorption of Mo(VI) on zirconium molybdosilicate gel and potential application as a 99Mo/99m Tc generator, Radiochemistry 58 (2016) 409–414.
[30] H.M. Aly, M.E. Moustafa, M.Y. Nassar, E.A. Abdelrahman, Synthesis and characterization of novel Cu (II) complexes with 3-substituted-4-amino-5-mercapto-1,2,4-triazole Schiff bases: a new route to CuO nanoparticles, J. Mol. Struct. 1086 (2015) 223–231.
[31] L. Zhao, Z. Liu, X. Zhang, T. Cui, J. Han, K. Guo, B. Wang, Y. Li, T. Hong, J. Liu, Z. Liu, Three-dimensional flower-like hybrid BiOI-zeolite composites with highly efficient adsorption and visible light photocatalytic activity, RSC Adv. 4 (2014) 45540–45547.
[32] S. Sadjadi, M.M. Heravi, Current advances in the utility of functionalized SBA mesoporous silica for developing encapsulated nanocatalysts: state of the art, RSC Adv. 7 (2017) 30815–30838.
[33] L. Emdadi, D.T. Tran, J. Zhang, W. Wu, H. Song, Q. Gan, D. Liu, Synthesis of titanosilicate pillared MFI zeolite as an efficient photocatalyst, RSC Adv. 7 (2017) 3249–3256.
[34] P. Kongkachuichay, S. Pimprom, Nafion/Analcime and Nafion/Faujasite composite membranes for polymer electrolyte membrane fuel cells, Chem. Eng. Res. Des. 88 (2010) 496–500.
[35] A. Potdar, A. Shukla, A. Kumar, Effect of gas phase modification of analcime zeolite composite membrane on separation of surfactant by ultrafiltration, J. Membr. Sci. 210 (2002) 209–225.

[36] Y. Kakutani, P. Weerachawanasak, Y. Hirata, M. Sano, T. Suzuki, T. Miyake, Highly effective K-Merlinoite adsorbent for removal of Cs+ and Sr2+ in aqueous solution, RSC Adv. 7 (2017) 30919–30928.
[37] M. Liu, D. An, L.-a. Hou, S. Yu, Y. Zhu, Zero valent iron particles impregnated zeolite X composites for adsorption of tetracycline in aquatic environment, RSC Adv. 5 (2015) 103480–103487.
[38] M. Khatamian, N. Khodakarampoor, M. Saket Oskoui, N. Kazemian, Synthesis and characterization of RGO/zeolite composites for the removal of arsenic from contaminated water, RSC Adv. 5 (2015) 35352–35360.
[39] H. Deng, Y. Ge, Formation of NaP zeolite from fused fly ash for the removal of Cu(ii) by an improved hydrothermal method, RSC Adv. 5 (2015) 9180–9188.
[40] S. Sen Gupta, K.G. Bhattacharyya, Adsorption of metal ions by clays and inorganic solids, RSC Adv. 4 (2014) 28537–28586.
[41] H. Runtti, P. Tynjälä, S. Tuomikoski, T. Kangas, T. Hu, J. Rämö, U. Lassi, Utilisation of barium-modified analcime in sulphate removal: isotherms, kinetics and thermodynamics studies, J. Water Process. Eng. 16 (2017) 319–328.
[42] S.N. Azizi, S. Ghasemi, M. Derakhshani-mansoorkuhi, The synthesis of analcime zeolite nanoparticles using silica extracted from stem of sorghum Halepenesic ash and their application as support for electrooxidation of formaldehyde, Int. J. Hydrog. Energy 41 (2016) 21181–21192.
[43] S.N. Azizi, S. Ehsani Tilami, Cu-modified analcime as a catalyst for oxidation of benzyl alcohol: experimental and theoretical, Microporous Mesoporous Mater. 167 (2013) 89–93.
[44] A. Bejar, S. Ben Chaabene, M. Jaber, J.-F. Lambert, L. Bergaoui, Mn-analcime: synthesis, characterization and application to cyclohexene oxidation, Microporous Mesoporous Mater. 196 (2014) 158–164.
[45] M.Y. Nassar, Size-controlled synthesis of CoCO3 and Co3O4 nanoparticles by free-surfactant hydrothermal method, Mater. Lett. 94 (2013) 112–115.
[46] M.Y. Nassar, I.S. Ahmed, Hydrothermal synthesis of cobalt carbonates using different counter ions: an efficient precursor to nano-sized cobalt oxide (Co3O4), Polyhedron 30 (2011) 2431–2437.
[47] M.Y. Nassar, T.Y. Mohamed, I.S. Ahmed, One-pot solvothermal synthesis of novel cobalt salicylaldimine–urea complexes: a new approach to Co3O4 nanoparticles, J. Mol. Struct. 1050 (2013) 81–87.
[48] P.N. Joshi, A. Thangaraj, V.P. Shiralkar, Studies on zeolite transformation of high-silica gmelinite into analcime, Zeolites 11 (1991) 164–168.
[49] B.S. Liu, D.C. Tang, C.T. Au, Fabrication of analcime zeolite fibers by hydrothermal synthesis, Microporous Mesoporous Mater. 86 (2005) 106–111.
[50] S. Naser Azizi, M. Yousefpour, Synthesis of aluminum-rich analcime using an ethylene diamine derivative as template, Z. Anorg. Allg. Chem. 635 (2009) 1654–1658.
[51] I.C. Lin, H.-J. Lo, S.-R. Song, J.-N. Fang, Y.-L. Chen, H.-F. Chen, L.-J. Li, C.-M. Liu, Controlling of solution concentration on nucleation during hydrothermal synthesis of analcime, J. Chin. Chem. Soc. 49 (2002) 495–498.
[52] Y.-y. Ge, Q. Tang, X.-m. Cui, Y. He, J. Zhang, Preparation of large-sized analcime single crystals using the Geopolymer-Gels-Conversion (GGC) method, Mater. Lett. 135 (2014) 15–18.
[53] A.Y. Atta, B.Y. Jibril, B.O. Aderemi, S.S. Adefila, Preparation of analcime from local kaolin and rice husk ash, Appl. Clay Sci. 61 (2012) 8–13.
[54] X. Ma, J. Yang, H. Ma, C. Liu, P. Zhang, Synthesis and characterization of analcime using quartz syenite powder by alkali-hydrothermal treatment, Microporous Mesoporous Mater. 201 (2015) 134–140.
[55] S.N. Azizi, M. Yousefpour, Synthesis of zeolites NaA and analcime using rice husk ash as silica source without using organic template, J. Mater. Sci. 45 (2010) 5692–5697.
[56] A.E. Ameh, O.O. Fatoba, N.M. Musyoka, L.F. Petrik, Influence of aluminium source on the crystal structure and framework coordination of Al and Si in fly ash-based zeolite NaA, Powder Technol. 306 (2017) 17–25.
[57] S.N. Azizi, S. Ghasemi, N.S. Gilani, An electrode with Ni(II) loaded analcime zeolite catalyst for the electrooxidation of methanol, Chin. J. Catal. 35 (2014) 383–390.
[58] N. Jaafar, H. Ben Rhaiem, A. Ben Haj Amara, Crystallographic, vibrational, thermal and electrochemical properties of nacrite-NH4Cl nanohybrid, Appl. Clay Sci. 132 (2016) 600–610.
[59] C.M. Manna, M.Y. Nassar, D. Tofan, K. Chakarawet, C.C. Cummins, Facile synthesis of mononuclear early transition-metal complexes of kappa3cyclo-tetrametaphosphate ([P4O12]4-) and cyclo-trimetaphosphate ([P3O9]3), Dalton Trans. 43 (2014) 1509–1518.
[60] M.Y. Nassar, A.S. Attia, S. Adawy, M.F. El-Shahat, Novel isatinoxime molybdenum and chromium complexes: synthesis, spectroscopic, and thermal characterization, J. Mol. Struct. 1026 (2012) 88–92.
[61] J. Yuan, J. Yang, H. Ma, C. Liu, C. Zhao, Hydrothermal synthesis of analcime and hydroxycancrinite from K-feldspar in Na2SiO3 solution: characterization and reaction mechanism, RSC Adv. 6 (2016) 54503–54509.
[62] M.Y. Nassar, I.S. Ahmed, T.Y. Mohamed, M. Khatab, A controlled, template-free, and hydrothermal synthesis route to sphere-like [small alpha]-Fe2O3 nanostructures for textile dye removal, RSC Adv. 6 (2016) 20001–20013.
[63] M.Y. Nassar, A.S. Amin, I.S. Ahmed, S. Abdallah, Sphere-like Mn2O3 nanoparticles: facile hydrothermal synthesis and adsorption properties, J. Taiwan Inst. Chem. Eng. 64 (2016) 79–88.
[64] M.Y. Nassar, A.S. Attia, K.A. Alfallous, M.F. El-Shahat, Synthesis of two novel dinuclear molybdenum(0) complexes of quinoxaline-2,3-dione: new precursors for preparation of α-MoO3 nanoplates, Inorg. Chim. Acta 405 (2013) 362–367.
[65] M.Y. Nassar, M. Khatab, Cobalt ferrite nanoparticles via a template-free hydrothermal route as an efficient nano-adsorbent for potential textile dye removal, RSC Adv. 6 (2016) 79688–79705.
[66] M.Y. Nassar, M.M. Moustafa, M.M. Taha, Hydrothermal tuning of the morphology and particle size of hydrozincite nanoparticles using different counterions to produce nanosized ZnO as an efficient adsorbent for textile dye removal, RSC Adv. 6 (2016) 42180–42195.
[67] H. Ticha, J. Schwarz, L. Tichy, On the structural arrangement and optical band gap (PbO)x(ZnO)10(TeO2)90—x glasses, J. Non-Cryst. Solids 459 (2017) 63–67.
[68] S. Zinatloo-Ajabshir, M. Salavati-Niasari, Facile route to synthesize zirconium dioxide (ZrO2) nanostructures: structural, optical and photocatalytic studies, J. Mol. Liq. 216 (2016) 545–551.
[69] S.K. Tripathy, A. Pattanaik, Optical and electronic properties of some semiconductors from energy gaps, Opt. Mater. 53 (2016) 123–133.